Development of an improved two-sphere integration technique for quantifying black carbon concentrations in the atmosphere and seasonal snow

Xin Wang [1, 2], **Xueying Zhang** [3] and **Wenjing Di** [1]

[1] Key Laboratory for Semi-Arid Climate Change of the Ministry of Education, Lanzhou University, Lanzhou 730000, Gansu, China

[2] Institute of Surface-Earth System Science, Tianjin University, Tianjin 300072

[3] Jilin Weather Modification Office, Changchun 132000, Jilin, China

Correspondence to: Xin Wang (Tel: +86 931 8915892)

E-mail address: wxin@lzu.edu.cn (X. Wang)

Submitted on August 2019

Abstract. An improved two-sphere integration (TSI) technique has been developed to quantify black carbon (BC) concentrations in the atmosphere and seasonal snow. The major advantage of this system is that it combines two distinct integrated-spheres to reduce the scattering effect due to light-absorbing particles, and thus provides accurate determinations of total light absorption from BC collected on Nuclepore filters. The TSI technique can be calibrated using a series of 15 filter samples of standard fullerene soot. This technique quantifies the mass of BC by separating the spectrally resolved total light absorption into BC and non-BC fractions. To assess the accuracy of the improved system, an empirical procedure for measuring BC concentrations by a two-step thermal–optical method is also applied. Laboratory results indicate that BC concentrations determined using the TSI technique and theoretical calculations are well correlated (R^2=0.99), whereas the thermal–optical method underestimates BC concentrations by 35%–45% than that measured by TSI technique. Assessments of the two methods for atmospheric and snow samples revealed excellent agreement, with least-squares regression lines with slopes of 1.72 (r^2 = 0.67) and 0.84 (r^2 = 0.93), respectively. However, the TSI technique is more accurate in quantifications of BC concentrations in both the atmosphere and seasonal snow, with an overall lower uncertainty. Using the improved TSI technique, we find that light absorption at a wavelength of 550 nm due to BC plays a dominant role, relative to non-BC light absorption, in both the atmosphere (62.76%–91.84% of total light absorption) and seasonal snow (43.11%–88.56%) over northern China.

ARTICLE INFO

Keywords:

Black carbon

Elemental carbon

Light absorption

Two-sphere integration technique

Thermal–optical method

1 Introduction

Black carbon (BC) has long been recognized as the major light-absorbing particles (LAPs) in both natural and anthropogenic emissions (Slater et al., 2002; Koch et al., 2009; Zhang et al., 2009; Pan et al., 2010; McMeeking et al., 2011; Pavese et al., 2012; Bond et al., 2013; IPCC, 2013). BC can impact the regional and global climate in several ways, including via the direct effects of scattering and absorbing visible solar radiation (Jacobson, 2001; Menon et al., 2002; Hansen et al., 2005; Ramanathan and Carmichael, 2008), the semi-direct effects of changing the temperature structure and relative humidity of the atmosphere by absorbing solar short-wave radiation (Ban-Weiss et al., 2012), and indirect effects on cloud formation and lifetime (Chuang et al., 2002; Baumgardner et al., 2004; Rosenfeld et al., 2008). Once deposited onto snow or ice surfaces, BC absorbs more solar radiation than pure snow or ice and reduces the snow albedo, thus accelerating snow melt (Xu et al., 2009a; Flanner et al., 2012; Hadley and Kirchstetter, 2012; Carmagnola et al., 2013; Qian et al., 2014; Zhao et al., 2014).

Optically classified BC is also often referred to as elemental carbon (EC), which is typically thermally detected. The distinction between BC and EC has been debated since the 1980s (Heintzenberg, 1989; Horvath, 1993a; Andreae and Gelencser, 2006; Moosmuller et al., 2009). Given that BC and EC are both soot particles with diameters of <1 μm, these terms have often been used interchangeably (Chow et al., 2001, 2004; Ming et al., 2009; Thevenon et al., 2009; Lim et al., 2014). BC is generally regarded as ideal light-absorbing particles of carbon, and is typically measured using optical attenuation methods (Clarke et al., 1967; Hansen et al., 1984; Ogren and Charlson, 1983; Grenfell et al., 2011). The term ‘EC’ is often used interchangeably with ‘BC’ when referring to optical absorption measurements (Clarke et al., 1967; Grenfell et al., 2011), and is only uniquely identified by thermal–optical methods (Xu et al., 2006; Cao et al., 2007; Jimenez et al., 2009). There remains poor agreement between measurements of BC and EC among available measurement techniques. The general techniques used to quantify the various fractions of BC mass concentrations are associated with the corresponding methods: thermal–optical methods, single-particle soot photometer (SP2) measurements, and filter-based optical techniques. Besides the above techniques, the aerosol mass

spectrometry, electron microscopy, and Raman spectroscopy are also useful and accurate methods to identify the various fractions of carbonaceous aerosols in the atmosphere (Ivleva et al., 2007; Spencer et al., 2007; Cross et al., 2010; Li et al., 2016; Petzold et al., 2013). Among these methods, the thermal–optical approach is regarded as the most effective and reliable for evaluating EC concentrations (Chylek et al., 1987; Cachier and Pertuisot, 1994; Jenk et al., 2006; Legrand et al., 2007; Hadley et al., 2010). However, the thermal–optical method can lead to large discrepancies in determining EC concentrations as a result of inference from positive artifacts caused by inadequately separated organics and mineral dust (Ballach et al., 2001; Wang et al., 2012). Further discrepancies are caused by the use of two main detection protocols [thermal–optical transmission (TOT) and thermal–optical reflectance (TOR)] to assess EC and OC concentrations based on their unique thermal properties. These protocols yield different OC and EC concentrations (Chow et al., 1993, 2001; Birch and Cary, 1996; Watson and Chow, 2002). The Integrating Sphere/Integrating Sandwich Spectrophotometer (ISSW) method was developed by Grenfell et al. (2011) and has been used to analyze mass concentrations of BC in snow (Doherty et al., 2010, 2014; Wang et al., 2013). Doherty et al. (2010) noted that the total uncertainty in measuring BC in snow using the ISSW method is up to 40% relative to the gravimetric standards of BC (fullerene soot). The total uncertainty associated with the filter-based ISSW technique on BC concentration determination for ambient snow has previously been estimated as 40 %, which is the sum, in quadrature, of 11% for instrumental uncertainty, 15% for undercatch uncertainty (loss of insoluble light-absorbing impurities), 17% for BC mass absorption coefficient (MAC) uncertainty, and 30% for uncertainty in the AAE of non-BC material (Doherty et al., 2010; Grenfell et al., 2011; Schwarz et al., 2012). Finally, the SP2 technique is well suited to the quantification of low BC concentrations with small particle radius (<500 nm). It is an optimized method for measuring BC concentrations and size distributions, and the substantially larger uncertainty of the SP2 instrument with respect to BC concentration measurements can exceed 60% in snow and ice cores, and 30% for atmospheric sampling (Schwarz et al., 2012). They noted that the relative transmission efficiencies of polystyrene latex sphere concentration standards (PSLs) in liquid to the SP2 after

aerosolization remarkably reduce to 20% due to larger diameter of BC particles (> 500 nm). Therefore, the larger diameter of BC (>500 nm) is hardly captured by SP2 instrument with a collison-type nebulizer. Moreover, the mixing status of BC in snow is more complicated than the standard fullerene soot in the laboratory and the typical BC in the atmosphere.

Although several field campaigns have collected atmospheric, snow, and ice core samples to measure BC and EC concentrations globally (Wolff and Cachier, 1998; von Schneidemesser et al., 2009; Doherty et al., 2010, 2014; Ming et al., 2010; Huang et al., 2011; Xu et al., 2012; Cong et al., 2015), biases remain in determinations of BC concentrations, as is evident from a comparison among the results obtained with the SP2, ISSW, and thermal–optical methods (Schwarz et al., 2012; Lim et al., 2014). As a result, it is difficult to assess the effects of BC and EC on recent climate change using different techniques, even in the same area.

Here we report the development of a new portable and accurate spectrophotometric method based on the two-sphere integration (TSI) technique that can be used to determine BC concentrations in both the atmosphere and seasonal snow. The improved TSI technique minimizes scattering effects related to BC and non-BC insoluble particles collected on Nuclepore filters, and thus provides a simple and accurate means to assess BC concentrations in the atmosphere and seasonal snow. To assess the accuracy of the new technique, a two-step thermal–optical method is applied to determine BC concentrations on individual quartz fiber filters. Finally, we investigate the spatial distribution of BC concentrations and the relative light absorption of surface snow over northeast China. We also analyze the diurnal variations of BC in the atmosphere during day and night over Lanzhou in northwest China.

2 Experimental Procedures

2.1 Sampling sites and snow-sample filtration

During the study period, less snow fell in 2014 than in 2010, and no seasonal snow was present in the western part of Inner Mongolia. Therefore, we collected 94 snow samples

at 14 sites in January and February of 2014 across north China following the sampling route of Huang et al. (2011). The sites are numbered in chronological order from 90 to 103, following previous snow surveys (Ye et al., 2012; Wang et al., 2013). Figure 1 shows the locations of the snow field campaigns across northern China. The sampling locations were selected to be at least 50 km from any settlement and 1 km from the nearest road. Snow samples were kept frozen before being filtered. We set up a temporary laboratory along the sampling route. Owing to BC in snow is often hydrophobic, long time melting could lose more BC to the container walls instead of collected on the filter (Ogren et al., 1983). In order to minimize the loss of insoluble ILAPs, we quickly melted the snow samples in a microwave within a very short time. Therefore, the loss of insoluble LAPs is very limited, and can be neglectable. At present, this method is widely performed for snow melting procedure. (Dothery et al., 2010, 2014; Wang et al.,2013). Subsequently, we simultaneously filtered the snow samples using quartz fiber filters with 1-μm pores and Nuclepore filters with 0.4-μm pores. Then, we refiltered the snow samples for the quartz fiber filters using Nuclepore filters with 0.4-μm pores to account for the loss of BC mass in the 1-μm pore quartz fiber filters. Finally, we stored the original and refiltered snow samples in clean high-density polyethylene bottles in a freezer at −30°C for subsequent analysis. For details of the sampling and filtration procedures, see Wang et al. (2013).

To evaluate the accuracy of the TSI technique in measuring BC concentrations, the atmospheric samples were collected continuously on Nuclepore and quartz fiber filters with high-volume samplers during the periods 09:00 to 17:00 (daytime; local time) and 23:00 to 07:00 (nighttime) at site 103 in Lanzhou from 5 to 25 August 2015. The pumps were operated at a flow rate of 10 L min^{-1}. In total, 40 atmospheric samples were collected during this experiment and used to assess the accuracy of the atmospheric BC concentration measurements of the improved TSI technique.

2.2 Two-sphere integration technique

Light transmission techniques are the most commonly used methods for determining light-absorbing impurities in aerosol filter samples of the atmosphere and snow/ice. Since the 1970s, a series of optical attenuation techniques have been developed for estimating

BC concentrations using light transmission changes through filters, based on Beer's law. An integrating sphere (IS) technique was first proposed for measuring BC by Fischer (1970). The integrating sphere was coated with diffusely reflecting white paint through a small hole, and the reduction in signal after measuring the sample filters represented the absorption of BC. Subsequently, a new integrating plate (IP) instrument was developed to measure scavenging BC on filters based on the IS technique, which uses a light-diffusing support to provide a nearly Lambertian light source for light transmission using 0.4-μm Nuclepore filters (Clarke et al., 1967; Horvath, 1993b). However, the multiple scattering of solar radiation affect the accuracy of the IP technique (Clarke et al., 1967; Hitzenberger, 1993; Petzold et al., 1997; Bond et al., 1999). A new integrating-sandwich configuration of the ISSW instrument was designed to measure the absorption of light-absorbing impurities based on the ISSW principle of Grenfell et al. (2011). The ISSW instrument can isolate the absorption properties of light-absorbing impurities deposited on polycarbonate Nuclepore filters. By assuming the mass absorption efficiency and non-BC Ångström exponent at 550 nm, this technique is currently capable of reliably measuring BC and non-BC light absorption (Wang et al., 2013; Dang and Hegg, 2014; Doherty et al., 2014). However, Schwarz et al. (2012) found that the total instrumental uncertainty associated with ISSW BC concentration determinations for ambient snow is 11%, and that this uncertainty is partially due to the scattering effects of insoluble impurities deposited on the filters (Doherty et al., 2010; Grenfell et al., 2011).

The improved TSI spectrophotometer developed in this study is small, lightweight, and portable, and can accurately quantify BC concentrations using a technique based on the integrating sphere and integrating plate transmission techniques (Fig. 2). The major improvement of this spectrophotometer is that we replaced the integrating sandwich of the ISSW instrument developed by Grenfell et al. (2011) with a new integrating sphere. In addition, an iron hoop is applied to the top integrating sphere surrounding the sapphire windows to reduce light scattering due to insoluble particles on the filters. Therefore, the total relative light absorption due to all insoluble impurities on the filter can be estimated from the visible-to-near-infrared wavelengths. The total light attenuation can be calculated from the light transmitted by a snow or atmospheric sample, $S(\lambda)$, compared

with that transmitted by a blank filter, $S_0(\lambda)$. Then, the relative attenuation (Atn) through the filter can be expressed as follows

$$Atn = -\ln[S(\lambda)/S_0(\lambda)] \quad (1)$$

Then, the total absorption Ångström exponent $Å_{tot}(\lambda_0)$ of all the ILAPs on the filters can be calculated from the following formula:

$$Å_{tot}(\lambda_0) = -\frac{\ln[\tau_{tot}(\lambda_1)/\tau_{tot}(\lambda_2)]}{\ln(\lambda_1/\lambda_2)} \quad (2)$$

$Å_{non-BC}$ is calculated as a linear combination of the contributions to light absorption made by OC and Fe:

$$Å_{non-BC} = Å_{OC} \times f_{OC} + Å_{Fe} \times f_{Fe} \quad (3)$$

The total absorption Ångström exponent of all ILAPs on a filter ($Å_{tot}$) can be described as a linear combination of $Å_{BC}$ and $Å_{non-BC}$ weighted by the light absorption fraction:

$$Å_{tot}(\lambda_0) = Å_{BC} \times f_{BC}(\lambda_0) + Å_{non-BC} \times f_{non-BC}(\lambda_0) \quad (4)$$

Using the mass absorption efficiency and absorption Ångström exponents for BC, OC, and Fe described by Wang et al. (2013), we can further estimate the following parameters: equivalent BC (C_{BC}^{equiv}), maximum BC (C_{BC}^{max}), estimated BC (C_{BC}^{est}), fraction of light absorption by non-BC ILAPs (insoluble light-absorbing particles) (f_{non-BC}^{est}), absorption Ångström exponent of non-BC ILAPs ($Å_{non\text{-}BC}$), and total absorption Ångström exponent ($Å_{tot}$). These parameters are defined as follows.

1. C_{BC}^{equiv} (ng g^{-1}): *equivalent BC* is the amount of BC that would be needed to produce the total light absorption by all insoluble particles in snow for wavelengths of 300–750 nm.

2. C_{BC}^{max} (ng g^{-1}): *maximum BC* is the maximum possible BC mixing ratio in snow, assuming that all light absorption is due to BC at wavelengths of 650–700 nm.

3. C_{BC}^{est} (ng g^{-1}): *estimated BC* is the estimated true mass of BC in snow derived by separating the spectrally resolved total light absorption and non-BC fractions.

4. f_{non-BC}^{est} (%): the *fraction of light absorption by non-BC light-absorbing particles* is the integrated absorption due to non-BC light-absorbing particles. This value is weighted by the down-welling solar flux at wavelengths of 300–750 nm.

5. $Å_{non\text{-}BC}$: the *non-BC absorption Ångström exponent* is derived from the light absorption by non-BC components for wavelengths of 450–600 nm.

6. $Å_{tot}$: the *absorption Ångström exponent* is calculated for all insoluble particles deposited on the filter between 450 and 600 nm.

Furthermore, combining with the mass loading of Fe was determined by chemical analysis (Wang et al., 2013), the mass loading of OC (L_{OC}) was also estimated assuming that the MAC for OC is 0.3 m^2 g^{-1} at the wavelength of 550 nm using the following equation:

$$\tau_{tot}(\lambda) - MAC_{BC}(\lambda) \times L_{BC}^{est} - MAC_{Fe} \times L_{Fe} = MAC_{OC} \times L_{OC} \qquad (5)$$

All relevant equations and associated derivations are described by Grenfell et al. (2011) and Doherty et al. (2010, 2014). Note that the calculation of non-BC light absorption due to insoluble impurities assumes that the iron in snow is predominantly from mineral dust (Wang et al., 2013).

2.3 Calibration of the TSI spectrophotometer

In this study, a series of 15 Nuclepore filters with a pore size of 0.2 μm (LOT# 7012284, 25mm, Whatman) loaded with fullerene soot (stock #40971, lot #L20W054, Alfa Aesar, Ward Hill, MA, USA) is used to calibrate the spectrophotometer over the range 0.63–38.6 μg, which typically covers >75% of ambient accumulation mode mass (left panel in Table 1; Schwarz et al., 2012). Fullerene soot is commonly used for calibrating the light transmission and thermal–optical techniques for measuring BC concentrations (Baumgardner et al., 2012). Standard fullerene soot particles are fractal-like aggregates of spherical primary particles with a diameter of ~50 nm, with a mean density of 1.05 g cm^{-3} (Moteki et al., 2009). Multiple filters with various loadings are required, as the system response deviates from Beer's law exponential behavior; related equations can be found in Grenfell et al. (2011). Note that uncertainties in mass absorption efficiencies, which range from 2 to 25 m^2 g^{-1}, can lead to uncertainty in this technique. Here, we use a mass absorption efficiency of 6.22 m^2 g^{-1} at 525 nm, which is consistent with Doherty et al. (2010) and Grenfell et al. (2011). Figure 3 shows the best-fit curve (solid line) of loading of the filters at 550 nm. When the filter loading was 0–40 μg cm^{-2}, all measured

results were close to the best-fit curve, indicating that the TSI spectrophotometer is stable and accurate in terms of BC mass measurements.

2.4 Thermal–optical measurements of EC concentration

There are several types of thermal–optical method that can be used to quantify EC and OC concentrations, including two-step temperatures in oxidizing/non-oxidizing atmospheres (Cachier et al., 1989; Xu et al., 2006, 2009b), thermal–optical reflectance (Chow et al., 1993, 2001; Chen et al., 2004), and thermal–optical transmittance (Sharma et al., 2002; Yang and Yu, 2002; Chow et al., 2004). Using an optimized two-step method, Cachier et al. (1989) first confirmed that soot carbon not only comprises EC, but is also mixed with highly condensed organic material. An optimized two-step thermal–optical system has been developed to detect EC and OC concentrations in ice cores (Xu et al., 2006). Here, we use the optimized two-step method based on the thermal–optical technique to measure EC concentrations. In this experiment, quartz fiber filters were first preheated in a muffle furnace at 350°C to remove organic carbon prior to sampling. All filters were punched to yield appropriately sized samples for analysis. Snow samples were analyzed for EC and OC concentrations using a Thermal–Optical Carbon Analyzer (Desert Research Institute, Model 2001A), following the thermal–optical reflectance (TOR) protocol of the Interagency Monitoring of Protected Visual Environments (IMPROVE_A). We developed a new method, referred to as the two-step method, to measure the concentrations of BC collected by the quartz fiber filters. The two-step method is an updated measurement procedure that first extracts an OC fraction below 550°C in a He atmosphere. The volatilized OC is oxidized to CO_2, reduced to CH_4, and detected by a flame ionization system. Next, two EC fractions (EC1 and EC2) are extracted above 550°C in an atmosphere of 2% O_2 and 98% He. Detailed procedures can be found in Xu et al. (2006) and Chow et al. (2004). The analytical uncertainty of this method is 15% for BC and 16% for OC measured via four parallel ice samples cut lengthways in an ice core with high dust loading (Xu et al., 2009a).

3 Results

3.1 Comparison with theoretical calculations

To further assess the accuracy of the TSI system, we use standard fullerene soot and quantify BC concentrations using theoretical calculations for comparison with BC values measured by a laboratory-based TSI spectrophotometer. To ensure the stability and accuracy of the improved TSI spectrophotometer, two individual sets of standard BC filters were used: 0.4-μm Nuclepore and 1-μm quartz fiber filters. All filters were preheated in a muffle furnace at 350°C to remove organic carbon prior to sampling. A measured amount of BC was mixed into a known volume of ultrapure water. The mixture was then agitated by ultrasound for ~10 min, and the same volumes of liquid were then filtered through the two types of filter. Using the calculated BC mass, seven filters with gradually increasing BC concentrations were obtained for both the 0.4-μm Nuclepore and 1-μm quartz fiber filters. Next, all the filters were placed in a dryer for 24 h and then measured using the TSI spectrophotometer. Using the BC mass and the volume of the ultrapure water used for filtration, we can estimate the theoretical BC concentration for each filter. The mass for each filter is listed in Table 1 (right panel).

Assuming a mass absorption cross-section (MAC) of BC of 6.22 m^2 g^{-1} at 525 nm, the BC concentrations measured using the TSI spectrophotometer were in good agreement with the theoretical BC values in the slope of 1.07 (Fig. 4). The BC mass loaded on the Nuclepore filters was approximately equal to that measured by the improved TSI spectrometer, which indicates that the TSI system developed here can accurately measure BC concentrations with the assumed mass absorption efficiency. In contrast, the standard BC mass on the quartz fiber filters was underestimated by 35%–45% using the two-step thermal–optical technique, compared with the theoretical value. During the filtration process, we found that the time required to filter liquid snow samples on the 0.4-μm Nuclepore filters was much longer than was the case for the 1-μm quartz fiber filters. Therefore, we first filtered the melted snow samples on the quartz fiber filters, and then re-filtered the snow samples using the 0.4-μm Nuclepore filters. Using this process, BC mass losses can be obtained using the TSI technique, assuming optical BC is equivalent to thermal EC.

As shown in Figure 5, the fraction of BC mass collected during the second filtration (0.4-μm filter) ranges from 12% to 21% of the total collected mass (filter directly with 0.4-μm filters), as might be expected for the small particles of standard fullerene soot (<50 nm). This under-sampled fraction decreases with increasing BC mass on the filters, possibly owing to blocking of the filter pores. As a result, the under-sampled fraction of the thermal–optical method was larger than that of the TSI technique, leading to a lower filtration efficiency. Note that these sampling efficiencies are strongly related to the BC size distribution. Therefore, the improved TSI technique developed here is more stable and accurate for measuring pure BC masses, and the data obtained using this method can be used as the standard BC mass. After correcting for systematic biases, the results of both methods were closer to the theoretical BC calculations. Note, however, that the size distribution of the laboratory BC standard was much smaller than those of the atmospheric and seasonal snow samples (Schwarz et al., 2012). Therefore, underestimates caused by the filtration efficiency for ambient BC should be lower than that for the standard BC.

3.2 Comparison of BC concentrations in seasonal snow and the atmosphere

Recent studies have indicated that mineral dust can affect the accurate detection of BC concentrations using the ISSW and thermal–optical methods (Wang et al., 2012; Zhou et al., 2017). To eliminate the large uncertainty and bias due to dust particles, we only used snow samples collected in industrial areas over northeastern China, where the light absorption was dominated by fine-mode ILAPs (e.g., BC and OC; Wang et al., 2013). Hence, most of the snow samples did not contain very large coarse-mode particles, such as mineral and local soil dust.

During the snow field campaign, two series of snow samples were filtered through the Nuclepore and quartz fiber filters and measured using the TSI and two-step thermal–optical methods (Fig. 6). Result shows that most of the BC values measured by the TSI and two-step thermal–optical methods are close to the 1:1 line in a comparison plot, and are generally in good agreement (slope of 1.11, $R^2 = 0.93$, n = 22). However, some BC values in seasonal snow measured by the two-step thermal–optical method are much larger than those measured by the TSI technique. Consequently, for each sample the

mean ratio of BC concentrations measured by the two-step method and the TSI spectrophotometer varies from 0.64 to 3.97, with an overall mean of 1.57. This discrepancy arises from two factors. First, Wang et al. (2017) found that snow grain sizes varied considerably (from 0.07 to 1.3 mm) during this snow field campaign. This range is much larger than that recorded in previous studies, owing to snow melting by solar radiation and ILAPs (Hadley and Kirchstetter, 2012; Painter et al., 2013; Yasunari et al., 2013; Pedersen et al., 2015). These results agree well with those of Schwarz et al. (2012), who found that the sizes of BC particles in snow are much larger than those in typical ambient air. Therefore, the sampling efficiency of the quartz fiber filters could have been significantly higher than expected. The other factor is that the insoluble light-absorbing impurities in seasonal snow over northeast China contained not only BC, but also insoluble organic carbon. This result is consistent with a previous study by Chow et al. (2004), who reported that the charring observed when employing the two-step thermal–optical method at higher temperatures (>550°C) was incomplete and that certain organic compounds are not completely pyrolyzed below 550°C. Therefore, incomplete charring of absorbed organic compounds by the two-step processes may lead to incompletely pyrolyzed OC on the filters, artificially contributing to the BC concentration. This may explain why the BC concentration measured using the thermal–optical method was higher than that measured using the TSI spectrophotometer.

A comparison of BC concentrations in the atmosphere measured by the ISSW and thermal–optical methods is vastly different than that for the snow samples (Fig. 7). Results are in excellent agreement for BC concentrations of < 3 μg m^{-3}. However, biases increased gradually with increasing BC concentrations, leading to two-step-to-TSI ratios as low as 0.5. The BC concentrations of > 3 μg m^{-3} obtained using the two-step thermal–optical method are much lower than those measured using the improved TSI technique, possibly due to the small particle sizes in the atmosphere, which lead to a lower filtration efficiency. Overall, we conclude that the improved TSI method is more stable and suitable for measuring BC concentrations in both the atmosphere and snow samples compared with the two-step thermal–optical method.

3.3 Spatial distribution of BC and non-BC light absorption measured by the TSI spectrophotometer

The above results show that the improved TSI method measures BC concentrations in the atmosphere and snow/ice with higher accuracy than Two-step thermal optical methods. In this section we investigate the spatial distribution of BC concentrations and their relative light absorption due to BC and non-BC snow impurities in seasonal snow over northeast China during January–February 2014. All BC mass concentrations in surface snow measured by the TSI and thermal–optical methods during the snow field campaigns are listed in Table 2. There was less snow fall in January 2014 than in 2010, and seasonal snow did not cover all of central Inner Mongolia during this time. Thus, we only collected snow samples at site 90. Given that this region is windy, the surface snow collected included drifted and aged snow. The surface BC concentration was 350 ng g^{-1} in the central Inner Mongolia region. The lowest BC concentrations in surface snow, 55 and 280 ng g^{-1}, were found on the border of northeast China (sites 91–97). We note that there were considerable variations in BC concentrations in these regions. The median BC concentration was 1100 ng g^{-1} with a range of 520–3900 ng g^{-1} for surface snow in northeast industrial regions. On 10 February 2014, fresh snow samples were collected in Lanzhou, at a mean snow depth of 6–8 cm. The mean BC concentration in these fresh snow samples from Lanzhou was ~170 ng g^{-1}.

The relative light absorption due to BC and non-BC fractions in seasonal snow measured using the improved TSI technique across northern China is shown in Figure 8. A similar pattern for the light absorption of BC (~70%) and non-BC (~30%) from insoluble light-absorbing impurities in surface snow indicates a similar pollution emission source over northeast China. However, the light absorption due to BC in seasonal snow plays a dominant role (43.11%–88.56%, with a mean of 73.10%). The largest BC light absorption was at site 102. This site is located in the central part of Jilin province, which is polluted by heavy industrial activity. For one sample, the light absorption of non-BC impurities in seasonal snow reached 56.89%, which is the only time it exceeded BC light-absorption. Biomass burning and fossil fuel are likely the major emission sources during the winter in Lanzhou, unlike the case over northeast

China. These results are consistent with those of Wang et al. (2013), who found that snow particle light absorption was dominated by BC in northeast China in 2010.

Finally, we investigate atmospheric BC mass concentrations and their relative light absorption measured by the TSI spectrophotometer in Lanzhou during 5–25 August 2015. During this experiment, there were no noticeable trends of BC concentrations in Lanzhou. However, a notable feature in Figure 9 is that the BC mass concentrations at night are generally much higher than during the day (Table 3). The unique topography of Lanzhou likely plays an important role in this phenomenon. Lanzhou is situated in a valley basin with low rainfall, high evaporation, low wind speeds, and high calm-wind frequency, which often leads to a thick inversion layer in which air pollutants accumulate during the night. The light absorption due to BC in the atmosphere ranges from 62.76% to 91.84%, with a mean of 75.43%.

4 Conclusions

We developed an improved two-sphere integration (TSI) spectrophotometer to quantify BC concentrations in snow and atmospheric samples over northern China. The TSI technique significantly reduces scattering effects caused by insoluble impurities deposited on filters. Therefore, the system more accurately measures light absorption due to BC and non-BC impurities. A system calibration using theoretical calculations for standard fullerene soot revealed that the TSI system can be used to assess BC concentrations with low uncertainty. A laboratory comparison revealed that the thermal–optical method can lead to a significant underestimate (35%–45%) of BC concentrations for small-diameter particles (~50 nm) due to the low filtration efficiency of 1-μm quartz fiber filters.

To further assess the accuracy of the improved TSI system, two field campaigns were carried out to collect seasonal snow and atmospheric samples during January–February 2014 and 5–25 August 2015 across northern China, respectively. Although the BC concentrations measured by the TSI and thermal–optical methods are well correlated for both the snow and atmospheric samples, we find that some BC values in seasonal snow measured by the two-step thermal–optical method were significantly overestimated compared with those measured by the TSI technique, by a factor of 1.57. Overall, the

improved TSI optical system developed here is applicable to quantifications of BC concentrations in the atmosphere and snow/ice.

The spatial distribution of BC concentrations in seasonal snow over northern China during January–February 2014 ranged from 60 to 3800 ng g^{-1}, with a mean value of 700 ng g^{-1}, and ranged from 0.78 to 7.75 μg m^{-3} in the atmosphere during 5–25 August 2015 in Lanzhou. The spatial distribution of BC concentrations shows that large BC values are found mainly in the center of industrial regions near the central part, whereas lower values are found in northeast China. Light absorption is dominated by BC (~40% to 90%) in seasonal snow over northeast China, and this plays a dominant role in accelerating snow melt. Atmospheric samples collected in Lanzhou show significant changes in BC concentrations between day and night. Frequent, stable atmospheric boundary layers at night during summer, caused by the valley-basin topography of Lanzhou, are largely responsible for air pollutant accumulation during the night.

Data availability. Data used in this paper are available upon request from corresponding author (wxin@lzu.edu.cn).

Author contributions. The conceptualization and methodology were done by XW. The experiments were designed by XZ and WD. The formal analysis, investigation, writing of the original draft, and editing were performed by XW.

Competing interests. The authors declare that they have no conflict of interest.

Acknowledgements. We thank Thomas C. Grenfell and Qiang Fu from University of Washington for providing the standard filters.

Financial support. This research was supported jointly by the National Key R&D Program of China (2019YFA0606801), the National Natural Science Foundation of

China (41975157, 41775144, 41675065, and 41875091), and the Fundamental Research Funds for the Central Universities (lzujbky-2018-k02).

References

Andreae, M.O. and Gelencser, A.: Black carbon or brown carbon? The nature of light-absorbing carbonaceous aerosols, Atmos. Chem. Phys., 6, 3131-3148, doi: 10.5194/acp-6-3131-2006, 2006.

Ban-Weiss, G.A., Cao, L., Bala, G., and Caldeira, K.: Dependence of climate forcing and response on the altitude of black carbon aerosols, Clim. Dyn., 38, 897-911, doi: 10.1007/s00382-011-1052-y, 2012.

Ballach, J., Hitzenberger, R., Schultz, E., and Jaeschke, W.: Development of an improved optical transmission technique for black carbon (BC) analysis, Atmos. Environ. , 35, 2089-2100, doi: 10.1016/S1352-2310(00)00499-4, 2001.

Baumgardner, D., Kok, G., and Raga, G.: Warming of the Arctic lower stratosphere by light absorbing particles, Geophys. Res. Lett., 31, doi: 10.1029/2003GL018883, 2004.

Baumgardner, D., Popovicheva, O., Allan, J., Bernardoni, V., Cao, J., Cavalli, F., Cozic, J., Diapouli, E., Eleftheriadis, K., Genberg, P.J., Gonzalez, C., Gysel, M., John, A., Kirchstetter, T.W., Kuhlbusch, T.A.J., Laborde, M., Lack, D., Muller, T., Niessner, R., Petzold, A., Piazzalunga, A., Putaud, J.P., Schwarz, J., Sheridan, P., Subramanian, R., Swietlicki, E., Valli, G., Vecchi, R., and Viana, M.: Soot reference materials for instrument calibration and intercomparisons: a workshop summary with recommendations, Atmos. Meas. Tech., 5, 1869-1887, doi: 10.5194/amt-5-1869-2012, 2012.

Birch, M. E., and Cary, R. A.: Elemental carbon-based method for monitoring occupational exposures to particulate diesel exhaust, Aerosol Sci. Technol., 25, 221-241, doi: 10.1080/02786829608965393, 1996.

490 Bond, T.C., Bussemer, M., Wehner, B., Keller, S., Charlson, R.J., and Heintzenberg, J.:
491 Light absorption by primary particle emissions from a lignite burning plant,
492 Environ. Sci. Technol., 33, 3887-3891, doi: 10.1021/es9810538, 1999.
493 Bond, T.C., Doherty, S.J., Fahey, D.W., Forster, P.M., Berntsen, T., DeAngelo, B.J.,
494 Flanner, M.G., Ghan, S., Karcher, B., Koch, D., Kinne, S., Kondo, Y., Quinn, P.K.,
495 Sarofim, M.C., Schultz, M.G., Schulz, M., Venkataraman, C., Zhang, H., Zhang, S.,
496 Bellouin, N., Guttikunda, S.K., Hopke, P.K., Jacobson, M.Z., Kaiser, J.W., Klimont, Z.,
497 Lohmann, U., Schwarz, J.P., Shindell, D., Storelvmo, T., Warren, S.G., and Zender,
498 C.S.: Bounding the role of black carbon in the climate system: A scientific
499 assessment, J. Geophys. Res.-Atmos., 118, 5380-5552, doi: 10.1002/jgrd.50171,
500 2013.
501 Cachier, H., Bremond, M.P., and Buat-Menard, P.: Determination of atmospheric soot
502 carbon with a simple thermal method, Tellus B., 41, 379-390, doi:
503 10.1111/j.1600-0889.1989.tb00316.x , 1989.
504 Cachier, H. and Pertuisot, M.H.: Particulate Carbon in Arctic Ice, Analusis, 22,
505 M34-M37, 1994.
506 Cao, J.J., Lee, S.C., Chow, J.C., Watson, J.G., Ho, K.F., Zhang, R.J., Jin, Z.D., Shen, Z.X., Chen,
507 G.C., Kang, Y.M., Zou, S.C., Zhang, L.Z., Qi, S.H., Dai, M.H., Cheng, Y., and Hu, K.:
508 Spatial and seasonal distributions of carbonaceous aerosols over China, J.
509 Geophys. Res.-Atmos., 112, doi: 10.1029/2006JD008205, 2007.
510 Carmagnola, C.M., Domine, F., Dumont, M., Wright, P., Strellis, B., Bergin, M., Dibb, J.,
511 Picard, G., Libois, Q., Arnaud, L., and Morin, S.: Snow spectral albedo at Summit,
512 Greenland: measurements and numerical simulations based on physical and
513 chemical properties of the snowpack, The Cryosphere, 7, 1139-1160, doi:
514 10.5194/tc-7-1139-2013, 2013.
515 Chen, L.W.A., Chow, J.C., Watson, J.G., Moosmuller, H., and Arnott, W.P.: Modeling
516 reflectance and transmittance of quartz-fiber filter samples containing elemental
517 carbon particles: Implications for thermal/optical analysis, J. Aerosol Sci., 35,
518 765-780, doi: 10.1016/j.jaerosci.2003.12.005, 2004.

519 Chow, J.C., Watson, J.G., Pritchett, L.C., Pierson, W.R., Frazier, C.A., and Purcell, R.G.:
520 The Dri Thermal Optical Reflectance Carbon Analysis System - Description,
521 Evaluation and Applications in United-States Air-Quality Studies, Atmos. Environ.,
522 27, 1185-1201, doi: 10.1016/0960-1686(93)90245-T , 1993.
523 Chow, J.C., Watson, J.G., Crow, D., Lowenthal, D.H., and Merrifield, T.: Comparison of
524 IMPROVE and NIOSH carbon measurements, Aerosol Sci. Technol., 34, 23-34, doi:
525 10.1080/02786820119073, 2001.
526 Chow, J.C., Watson, J.G., Chen, L.W.A., Arnott, W.P., Moosmuller, H., and Fung, K.:
527 Equivalence of elemental carbon by thermal/optical reflectance and
528 transmittance with different temperature protocols, Environ. Sci. Technol., 38,
529 4414-4422, doi: 10.1021/es034936u, 2004.
530 Chuang, C.C., Penner, J.E., Prospero, J.M., Grant, K.E., Rau, G.H., and Kawamoto, K.:
531 Cloud susceptibility and the first aerosol indirect forcing: Sensitivity to black
532 carbon and aerosol concentrations, J. Geophys. Res.-Atmos., 107, doi:
533 10.1029/2000JD000215, 2002.
534 Chylek, P., Srivastava, V., Cahenzli, L., Pinnick, R.G., Dod, R.L., Novakov, T., Cook, T.L.,
535 and Hinds, B.D.: Aerosol and Graphitic Carbon Content of Snow, J. Geophys.
536 Res.-Atmos., 92, 9801-9809, doi: 10.1029/JD092iD08p09801, 1987.
537 Clarke, A.D., Noone, K.J., Heintzenberg, J., Warren, S.G., and Covert, D.S.: Aerosol
538 Light-Absorption Measurement Techniques - Analysis and Intercomparisons,
539 Atmos. Environ., 21, 1455-1465, doi: 10.1016/0004-6981(67)90093-5, 1967.
540 Cong, Z., Kang, S., Kawamura, K., Liu, B., Wan, X., Wang, Z., Gao, S., and Fu, P.:
541 Carbonaceous aerosols on the south edge of the Tibetan Plateau: concentrations,
542 seasonality and sources, Atmos. Chem. Phys., 15, 1573-1584, doi:
543 10.5194/acp-15-1573-2015, 2015.
544 Cross, E.S., Onasch, T.B., Ahern, A., Wrobel, W., Slowik, J.G., Olfert, J., Lack, D.A.,
545 Massoli, P., Cappa, C.D., Schwarz, J.P., Spackman, J.R., Fahey, D.W., Sedlacek, A.,
546 Trimborn, A., Jayne, J.T., Freedman, A.,Williams, L.R., Ng, N.L., Mazzoleni, C., Dubey,
547 M., Brem, B., Kok, G., Subramanian, R., Freitag, S., Clarke, A., Thornhill, D., Marr,
548 L.C., Kolb, C.E., Worsnop, D.R., and Davidovits, P.: Soot Particle Studies-Instrument

549 Inter-Comparison-Project Overview, Aerosol Sci. Technol., 44, 592–611, 2010.
550 Dang, C. and Hegg, D.A.: Quantifying light absorption by organic carbon in Western
551 North American snow by serial chemical extractions, J. Geophys. Res.-Atmos., 119,
552 10247-10261, doi: 10.1002/2014JD022156, 2014.
553 Doherty, S.J., Warren, S.G., Grenfell, T.C., Clarke, A.D., and Brandt, R.E.:
554 Light-absorbing impurities in Arctic snow, Atmos. Chem. Phys., 10, 11647-11680,
555 doi: 10.5194/acp-10-11647-2010, 2010.
556 Doherty, S.J., Dang, C., Hegg, D.A., Zhang, R.D., and Warren, S.G.: Black carbon and
557 other light-absorbing particles in snow of central North America, J. Geophys.
558 Res.-Atmos., 119, 12807-12831, doi: 10.1002/2014JD022350, 2014.
559 Fischer K.: Bestimmung der Absorption von sichtbarer Strahlung durch
560 Aerosolpartikeln, Contr. Atmos. Phys., 43, 244-254, 1970.
561 Flanner, M.G., Liu, X., Zhou, C., Penner, J.E., and Jiao, C.: Enhanced solar energy
562 absorption by internally-mixed black carbon in snow grains, Atmos. Chem. Phys.,
563 12, 4699-4721, doi: 10.5194/acp-12-4699-2012, 2012.
564 Grenfell, T.C., Doherty, S.J., Clarke, A.D., and Warren, S.G.: Light absorption from
565 particulate impurities in snow and ice determined by spectrophotometric
566 analysis of filters, Appl. Opt., 50, 2037-2048, doi: 10.1364/AO.50.002037, 2011.
567 Hadley, O.L., Corrigan, C.E., Kirchstetter, T.W., Cliff, S.S., and Ramanathan, V.:
568 Measured black carbon deposition on the Sierra Nevada snow pack and
569 implication for snow pack retreat, Atmos. Chem. Phys., 10, 7505-7513, doi:
570 10.5194/acp-10-7505-2010, 2010.
571 Hadley, O.L. and Kirchstetter, T.W.: Black-carbon reduction of snow albedo, Nat.
572 Clim. Chang., 2, 437-440, doi: 10.1038/NCLIMATE1433, 2012.
573 Hansen, A. D. A., Rosen, H., and Novakov, T.: The aethalometer — An instrument for
574 the real-time measurement of optical absorption by aerosol particles, Sci. Total
575 Environ., 36, 191-196, doi: 10.1016/0048-9697(84)90265-1, 1984.
576 Hansen, J., Sato, M., Ruedy, R., Nazarenko, L., Lacis, A., Schmidt, G.A., Russell, G.,
577 Aleinov, I., Bauer, M., Bauer, S., Bell, N., Cairns, B., Canuto, V., Chandler, M., Cheng,
578 Y., Del Genio, A., Faluvegi, G., Fleming, E., Friend, A., Hall, T., Jackman, C., Kelley, M.,

579 Kiang, N., Koch, D., Lean, J., Lerner, J., Lo, K., Menon, S., Miller, R., Minnis, P.,
580 Novakov, T., Oinas, V., Perlwitz, J., Perlwitz, J., Rind, D., Romanou, A., Shindell, D.,
581 Stone, P., Sun, S., Tausnev, N., Thresher, D., Wielicki, B., Wong, T., Yao, M., and
582 Zhang, S.: Efficacy of climate forcings, J. Geophys. Res.-Atmos., 110, doi:
583 10.1029/2005JD005776, 2005.
584 Heintzenberg, J.: Fine particles in the global troposphere A review, Tellus B., 41,
585 149-160, doi: 10.1111/j.1600-0889.1989.tb00132.x, 1989.
586 Hitzenberger, R.: Absorption-Measurements with an Integrating Plate Photometer
587 Calibration and Error Analysis, Aerosol Sci. Technol., 18, 70-84, doi:
588 10.1080/02786829308959585, 1993.
589 Horvath, H.: Comparison of Measurements of Aerosol Optical-Absorption by Filter
590 Collection and a Transmissometric Method, Atmos. Environ., 27, 319-325, doi:
591 10.1016/0960-1686(93)90105-8, 1993a.
592 Horvath, H.: Atmospheric Light-Absorption - a Review, Atmos. Environ., 27, 293-317,
593 doi: 10.1016/0960-1686(93)90104-7, 1993b.
594 Huang, J.P., Fu, Q.A., Zhang, W., Wang, X., Zhang, R.D., Ye, H., and Warren, S.G.: Dust
595 and Black Carbon in Seasonal Snow across Northern China, Bull. Amer. Meteor.
596 Soc., 92, 175-181, doi: 10.1175/2010BAMS3064.1, 2011.
597 IPCC. 2013. Climate Change 2013: The Physical Science Basis[M]. Stocker, T. F., D .
598 Qin, G. K. Plattner, et al., Cambridge, United Kingdom and New York, NY, USA.
599 Ivleva, N. P., McKeon, U., Niessner, R., and Pöschl, U.: Raman microspectroscopic
600 analysis of size-resolved atmospheric aerosol particle samples collected with an
601 ELPI: Soot, humic-like substances, and inorganic compounds, Aerosol Sci.
602 Technol., 41, 655–671, doi:10.1080/02786820701376391, 2007.
603 Jacobson, M.Z.: Global direct radiative forcing due to multicomponent anthropogenic
604 and natural aerosols, J. Geophys. Res.-Atmos., 106, 1551-1568, doi:
605 10.1029/2000JD900514, 2001.
606 Jenk, T.M., Szidat, S., Schwikowski, M., Gaggeler, H.W., Brutsch, S., Wacker, L., Synal,
607 H.A., and Saurer, M.: Radiocarbon analysis in an Alpine ice core: record of
608 anthropogenic and biogenic contributions to carbonaceous aerosols in the past

609 (1650-1940), Atmos. Chem. Phys., 6, 5381-5390, doi: 10.5194/acp-6-5381-2006,
610 2006.
611 Jimenez, J. L., Canagaratna, M. R., Donahue, N. M., Prevot, A.S.H., Zhang, Q., Kroll, J.H.,
612 DeCarlo, P.F., Allan, J.D., Coe, H., Ng, N.L., Aiken, A.C., Docherty, K.S., Ulbrich, I.M.,
613 Grieshop, A.P., Robinson, A.L., Duplissy, J., Smith, J.D., Wilson, K.R., Lanz, V.A.,
614 Hueglin, C., Sun, Y.L., Tian, J., Laaksonen, A., Raatikainen, T., Rautiainen, J.,
615 Vaattovaara, P., Ehn, M., Kulmala, M., Tomlinson, J.M., Collins, D.R., Cubison, M.J.,
616 Dunlea, E.J., Huffman, J.A., Onasch, T.B., Alfarra, M.R., Williams, P.I., Bower, K.,
617 Kondo, Y., Schneider, J., Drewnick, F., Borrmann, S., Weimer, S., Demerjian, K.,
618 Salcedo, D., Cottrell, L., Griffin, R., Takami, A., Miyoshi, T., Hatakeyama, S., Shimono,
619 A., Sun, J.Y., Zhang, Y.M., Dzepina, K., Kimmel, J.R., Sueper, D., Jayne, J.T., Herndon,
620 S.C., Trimborn, A.M., Williams, L.R., Wood, E.C., Middlebrook, A.M., Kolb, C.E.,
621 Baltensperger, U., Worsnop, D.R.: Evolution of organic aerosols in the atmosphere,
622 Science, 326, 1525–1529, 2009.
623 Koch, D., Schulz, M., Kinne, S., McNaughton, C., Spackman, J.R., Balkanski, Y., Bauer, S.,
624 Berntsen, T., Bond, T.C., Boucher, O., Chin, M., Clarke, A., De Luca, N., Dentener, F.,
625 Diehl, T., Dubovik, O., Easter, R., Fahey, D.W., Feichter, J., Fillmore, D., Freitag, S.,
626 Ghan, S., Ginoux, P., Gong, S., Horowitz, L., Iversen, T., Kirkevag, A., Klimont, Z.,
627 Kondo, Y., Krol, M., Liu, X., Miller, R., Montanaro, V., Moteki, N., Myhre, G., Penner,
628 J.E., Perlwitz, J., Pitari, G., Reddy, S., Sahu, L., Sakamoto, H., Schuster, G., Schwarz,
629 J.P., Seland, O., Stier, P., Takegawa, N., Takemura, T., Textor, C., van Aardenne, J.A.,
630 and Zhao, Y.: Evaluation of black carbon estimations in global aerosol models,
631 Atmos. Chem. Phys., 9, 9001-9026, doi: 10.5194/acp-9-9001-2009, 2009.
632 Legrand, M., Preunkert, S., Schock, M., Cerqueira, M., Kasper-Giebl, A., Afonso, J., Pio,
633 C., Gelencser, A., and Dombrowski-Etchevers, I.: Major 20th century changes of
634 carbonaceous aerosol components (EC, WinOC, DOC, HULIS, carboxylic acids, and
635 cellulose) derived from Alpine ice cores, J. Geophys. Res.-Atmos., 112, doi:
636 10.1029/2006JD008080, 2007.
637 Li, W., Shao, L., Zhang, D., Ro, C.-U., Hu, M., Bi, X., Geng, H., Matsuki, A., Niu, H., and
638 Chen, J.: A review of single aerosol particle studies in the atmosphere of East Asia:

morphology, mixing state, source, and heterogeneous reactions, J. Clean Prod., 112, 1330-1349, https://doi.org/10.1016/j.jclepro.2015.04.050, 2016.

Lim, S., Fain, X., Zanatta, M., Cozic, J., Jaffrezo, J.L., Ginot, P., and Laj, P.: Refractory black carbon mass concentrations in snow and ice: method evaluation and inter-comparison with elemental carbon measurement, Atmos. Meas. Tech., 7, 3307-3324, doi: 10.5194/amt-7-3307-2014, 2014.

McMeeking, G.R., Morgan, W.T., Flynn, M., Highwood, E.J., Turnbull, K., Haywood, J., and Coe, H.: Black carbon aerosol mixing state, organic aerosols and aerosol optical properties over the United Kingdom, Atmos. Chem. Phys., 11, 9037-9052, doi: 10.5194/acp-11-9037-2011, 2011.

Menon, S., Hansen, J., Nazarenko, L., Luo, Y.F.: Climate effects of black carbon aerosols in China and India, Science 297, 2250-2253, doi: 10.1126/science.1075159, 2002.

Ming, J., Xiao, C.D., Cachier, H., Qin, D.H., Qin, X., Li, Z.Q., and Pu, J.C.: Black Carbon (BC) in the snow of glaciers in west China and its potential effects on albedos, Atmos. Res., 92, 114-123, doi: 10.1016/j.atmosres.2008.09.007, 2009.

Ming, J., Xiao, C.D., Sun, J.Y., Kang, S.C., and Bonasoni, P.: Carbonaceous particles in the atmosphere and precipitation of the Nam Co region, central Tibet, J. Environ. Sci., 22, 1748-1756, doi: 10.1016/S1001-0742(09)60315-6, 2010.

Moosmuller, H., Chakrabarty, R.K., and Arnott, W.P.: Aerosol light absorption and its measurement: A review, J. Quant. Spectrosc. Ra., 110, 844-878, doi: 10.1016/j.jqsrt.2009.02.035, 2009.

Moteki, N., Kondo, Y., Takegawa, N., and Nakamura, S.-i.: Directional dependence of thermal emission from nonspherical carbon particles, J. Aerosol Sci., 40, 790-801, doi: 10.1016/j.jaerosci.2009.05.003, 2009.

Ogren, J. A. and Charlson, R. J.: Elemental carbon in the atmosphere– cycle and lifetime, Tellus, 35B, 241–254, 1983.

Painter, T.H., Seidel, F.C., Bryant, A.C., Skiles, S.M., and Rittger, K.: Imaging spectroscopy of albedo and radiative forcing by light-absorbing impurities in

668 mountain snow, J. Geophys. Res.-Atmos., 118, 9511-9523, doi:
669 10.1002/jgrd.50520, 2013.
670 Pan, Y.P., Wang, Y.S., Xin, J.Y., Tang, G.Q., Song, T., Wang, Y.H., Li, X.R., and Wu, F.K.:
671 Study on dissolved organic carbon in precipitation in Northern China, Atmos.
672 Environ., 44, 2350-2357, doi: 10.1016/j.atmosenv.2010.03.033, 2010.
673 Pavese, G., Calvello, M., and Esposito, F.: Black Carbon and Organic Components in
674 the Atmosphere of Southern Italy: Comparing Emissions from Different Sources
675 and Production Processes of Carbonaceous Particles, Aerosol Air Qual. Res., 12,
676 1146-1156, doi: 10.4209/aaqr.2011.12.0236, 2012.
677 Pedersen, C.A., Gallet, J.C., Strom, J., Gerland, S., Hudson, S.R., Forsstrom, S., Isaksson,
678 E., and Berntsen, T. K.: In situ observations of black carbon in snow and the
679 corresponding spectral surface albedo reduction, J. Geophys. Res.-Atmos., 120,
680 1476-1489, doi: 10.1002/2014jd022407, 2015.
681 Petzold, A., Kopp, C., and Niessner, R.: The dependence of the specific attenuation
682 cross-section on black carbon mass fraction and particle size, Atmos. Environ., 31,
683 661-672, doi: 10.1016/S1352-2310(96)00245-2, 1997.
684 Petzold, A., Ogren, J. A., Fiebig, M., Laj, P., Li, S.-M., Baltensperger, U., Holzer-Popp, T.,
685 Kinne, S., Pappalardo, G., Sugimoto, N., Wehrli, C., Wiedensohler, A., and Zhang,
686 X.-Y.: Recommendations for reporting "black carbon" measurements, Atmos.
687 Chem. Phys., 13, 8365-8379, https://doi.org/10.5194/acp-13-8365-2013, 2013.
688 Qian, Y., Wang, H., Zhang, R., Flanner, M.G., and Rasch, P.J.: A sensitivity study on
689 modeling black carbon in snow and its radiative forcing over the Arctic and
690 Northern China, Environ. Res. Lett., 9, 064001, doi:
691 10.1088/1748-9326/9/6/064001, 2014.
692 Ramanathan, V., and Carmichael, G.: Global and regional climate changes due to
693 black carbon, Nat. Geosci. , 1, 221-227, Doi 10.1038/Ngeo156, 2008.
694 Rosenfeld, D., Lohmann, U., Raga, G.B., O'Dowd, C.D., Kulmala, M., Fuzzi, S., Reissell, A.,
695 and Andreae, M.O.: Flood or drought: How do aerosols affect precipitation?
696 Science 321, 1309-1313, doi: 10.1126/science.1160606, 2008.

697 Schwarz, J.P., Doherty, S.J., Li, F., Ruggiero, S.T., Tanner, C.E., Perring, A.E., Gao, R.S.,
698 and Fahey, D.W.: Assessing Single Particle Soot Photometer and Integrating
699 Sphere/Integrating Sandwich Spectrophotometer measurement techniques for
700 quantifying black carbon concentration in snow, Atmos. Meas. Tech., 5,
701 2581-2592, doi: 10.5194/amt-5-2581-2012, 2012.
702 Sharma, S., Brook, J.R., Cachier, H., Chow, J., Gaudenzi, A., and Lu, G.: Light absorption
703 and thermal measurements of black carbon in different regions of Canada, J.
704 Geophys. Res.-Atmos., 107, doi: 10.1029/2002JD002496, 2002.
705 Slater, J.F., Currie, L.A., Dibb, J.E., and Benner, B.A.: Distinguishing the relative
706 contribution of fossil fuel and biomass combustion aerosols deposited at Summit,
707 Greenland through isotopic and molecular characterization of insoluble carbon,
708 Atmos. Environ., 36, 4463-4477, doi: 10.1016/S1352-2310(02)00402-8, 2002.
709 Spencer, M.T., Shields, L.G., and Prather, K. A.: Simultaneous measurement of the
710 effective density and chemical composition of ambient aerosol particles, Environ.
711 Sci. Technol., 41, 1303–1309, doi:10.1021/es061425+, 2007.
712 Thevenon, F., Anselmetti, F.S., Bernasconi, S.M., and Schwikowski, M.: Mineral dust
713 and elemental black carbon records from an Alpine ice core (Colle Gnifetti glacier)
714 over the last millennium, J. Geophys. Res.-Atmos., 114, doi:
715 10.1029/2008JD011490, 2009.
716 von Schneidemesser, E., Schauer, J.J., Hagler, G.S.W., and Bergin, M.H.:
717 Concentrations and sources of carbonaceous aerosol in the atmosphere of Summit,
718 Greenland, Atmos. Environ., 43, 4155-4162, doi: 10.1016/j.atmosenv.2009.05.043,
719 2009.
720 Wang, M., Xu, B., Zhao, H., Cao, J., Joswiak, D., Wu, G., and Lin, S.: The Influence of
721 Dust on Quantitative Measurements of Black Carbon in Ice and Snow when Using
722 a Thermal Optical Method, Aerosol Sci. Technol., 46, 60-69, doi:
723 10.1080/02786826.2011.605815, 2012.
724 Wang, X., Doherty, S.J., and Huang, J.P.: Black carbon and other light-absorbing
725 impurities in snow across Northern China, J. Geophys. Res.-Atmos., 118,
726 1471-1492, doi: 10.1029/2012JD018291, 2013.

727 Wang, X., Pu, W., Ren, Y., Zhang, X.L., Zhang, X.Y., Shi, J.S., Jin, H.C., Dai, M.K., Chen, Q.L.:
728 Observations and model simulations of snow albedo reduction in seasonal snow
729 due to insoluble light-absorbing particles during 2014 Chinese survey, Atmos.
730 Chem. Phys., 17, 2279-2296, doi: 10.5194/acp-17-2279-2017, 2017.
731 Watson, J. G., and Chow, J. C.: Comparison and evaluation of in situ and filter carbon
732 measurements at the Fresno Supersite, J. Geophys. Res.-Atmos., 107,
733 doi:10.1029/2001jd000573, 2002.
734 Wolff, E.W. and Cachier, H.: Concentrations and seasonal cycle of black carbon in
735 aerosol at a coastal Antarctic station, J. Geophys. Res.-Atmos., 103, 11033-11041,
736 doi: 10.1029/97JD01363, 1998.
737 Xu, B.Q., Yao, T.D., Liu, X.Q., and Wang, N.L.: Elemental and organic carbon
738 measurements with a two-step heating-gas chromatography system in snow
739 samples from the Tibetan Plateau, Annals of Glaciology, Vol 43, 2006 43, 257-262,
740 doi: 10.3189/172756406781812122, 2006.
741 Xu, B.Q., Cao, J.J., Hansen, J., Yao, T.D., Joswia, D.R., Wang, N.L., Wu, G.J., Wang, M.,
742 Zhao, H.B., Yang, W., Liu, X.Q., and He, J.Q.: Black soot and the survival of Tibetan
743 glaciers, Proc. Nat. Acad. Sci. U.S.A., 106, 22114-22118, doi:
744 10.1073/pnas.0910444106, 2009a.
745 Xu, B.Q., Wang, M., Joswiak, D.R., Cao, J.J., Yao, T.D., Wu, G.J., Yang, W., and Zhao, H.B.:
746 Deposition of anthropogenic aerosols in a southeastern Tibetan glacier, J. Geophys.
747 Res.-Atmos., 114, doi: 10.1029/2008JD011510, 2009b.
748 Xu, B.Q., Cao, J.J., Joswiak, D.R., Liu, X.Q., Zhao, H.B., and He, J.Q.: Post-depositional
749 enrichment of black soot in snow-pack and accelerated melting of Tibetan glaciers,
750 Environ. Res. Lett., 7, doi: 10.1088/1748-9326/7/1/014022, 2012.
751 Yang, H., and Yu, J.Z.: Uncertainties in charring correction in the analysis of
752 elemental and organic carbon in atmospheric particles by thermal/optical
753 methods, Environ. Sci. Technol., 36, 5199-5204, doi: 10.1021/es025672z , 2002.
754 Yasunari, T. J., Tan, Q., Lau, K. M., Bonasoni, P., Marinoni, A., Laj, P., Menegoz, M.,
755 Takemura, T., and Chin, M.: Estimated range of black carbon dry deposition and
756 the related snow albedo reduction over Himalayan glaciers during dry

pre-monsoon periods, Atmos. Environ., 78, 259-267, doi:10.1016/j.atmosenv.2012.03.031, 2013.

Ye, H., Zhang, R.D., Shi, J.S., Huang, J.P., Warren, S.G., and Fu, Q.: Black carbon in seasonal snow across northern Xinjiang in northwestern China, Environ. Res. Lett., 7, doi: 10.1088/1748-9326/7/4/044002, 2012.

Zhang, R.J., Ho, K.F., Cao, J.J., Han, Z.W., Zhang, M.G., Cheng, Y., and Lee, S.C.: Organic carbon and elemental carbon associated with PM10 in Beijing during spring time, J. Hazard. Mater., 172, 970-977, doi: 10.1016/j.jhazmat.2009.07.087, 2009.

Zhao, C., Hu, Z., Qian, Y., Leung, L.R., Huang, J., Huang, M., Jin, J., Flanner, M.G., Zhang, R., Wang, H., Yan, H., Lu, Z., and Streets, D.G.: Simulating black carbon and dust and their radiative forcing in seasonal snow: a case study over North China with field campaign measurements, Atmos. Chem. Phys., 14, 11475-11491, doi: 10.5194/acp-14-11475-2014, 2014.

Zhou, Y., Wang, X., Wu, X.Q., Cong, Z.Y., Wu, G.M., Ji, M.X.: Quantifying Light Absorption of Iron Oxides and Carbonaceous Aerosol in Seasonal Snow across Northern China, Atmosphere-Basel, 8, doi: 10.3390/atmos8040063, 2017.

Figure captions:

Figure 1 Sampling locations. Sites 90–102 are located in northeast China and were used for snow sample collection during Jan–Feb. 2014. Snow sampling site 103 is located in Lanzhou in northwest China, and was used for atmospheric sample collection during 5–25 August 2015. Sites are numbered according to Wang et al. (2013) and Ye et al. (2012).

Figure 2 Schematic diagram of the improved two-sphere integrating spectrophotometer.

Figure 3 Calibration curve for standard fullerene soot at a wavelength of 550 nm. The solid line is a best-fit curve for the filter measurements. S_0 and S are the detected signals for the blank and sample filters, respectively, and $-\ln(S/S_0)$ is the relative attenuation.

Figure 4 Comparison of the theoretical and measured BC mass determined by the TSI and two-step techniques in the laboratory. The solid and dot–dashed lines represent best-fit lines for the TSI and two-step techniques, respectively. The dashed line is a 1:1 line.

Figure 5 Mass loss of standard fullerene soot on 1.0-μm quartz fiber filters determined by refiltration using 0.4-μm Nuclepore filters.

Figure 6 Comparison of BC concentrations in snow samples over northeast China during January–February 2014 determined by the TSI and two-step thermal optical methods. A 1:1 line (dashed) is shown.

Figure 7 As for Fig. 6, but for atmospheric samples collected at Lanzhou in northwest China during 5–25 August 2015. A 1:1 line (dashed) and a linear regression fit passing through the origin (solid curve) are also shown.

Figure 8 Spatial distributions of light absorption at 550 nm due to BC and non-BC fractions in surface

796 snow across northern China during January–February 2014.

797 Figure 9 Variations in 8-hour (a) BC concentration and (b) BC and non-BC light absorption measured

798 by TSI spectrophotometer at 550 nm at Lanzhou during 5–25 August 2015 (day: 9 am to 5 pm; night:

799 11 pm to 7 am).

800

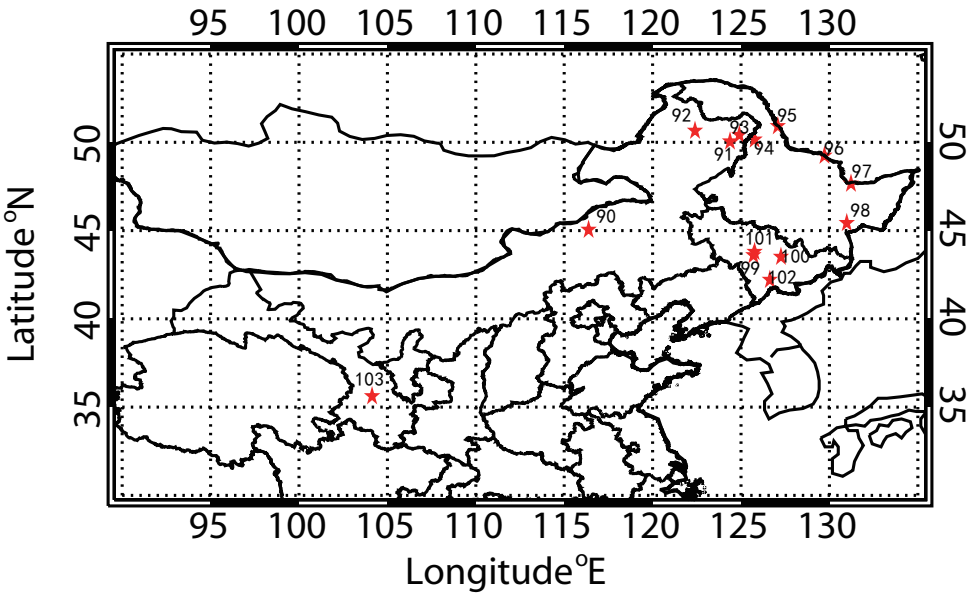

801

802 **Figure 1** Sampling locations. Sites 90–102 are located in northeast China and were used
803 for snow sample collection during Jan–Feb. 2014. Snow sampling site 103 is located in
804 Lanzhou in northwest China, and was used for atmospheric sample collection during 5–
805 25 August 2015. Sites are numbered according to Wang et al. (2013) and Ye et al. (2012).

806

807 **Table 1** Series of 15 standard filters loaded with fullerene soot, and a comparison of BC
808 concentrations between theoretical calculations and the TSI/two-step thermal–optical
809 methods in the laboratory.

Filter	Standard BC Concentration ($\mu g/cm^2$)	Filter	Standard BC Concentration ($\mu g/cm^2$)	Filter	Calculated BC (μg)	TSI BC (μg)	Two-step BC (μg)
1	0.63	9	2.82	1	3.68	3.92	2.28
2	0.70	10	3.65	2	10.58	11.39	5.86
3	0.78	11	5.53	3	17.48	17.49	11.39
4	0.86	12	6.35	4	24.38	24.94	15.67
5	0.93	13	12.5	5	31.28	32.52	18.07
6	1.33	14	19.00	6	38.18	39.14	24.29
7	2.12	15	38.6	7	45.08	49.18	28.61
8	2.49	-	-	-	-	-	

810
811

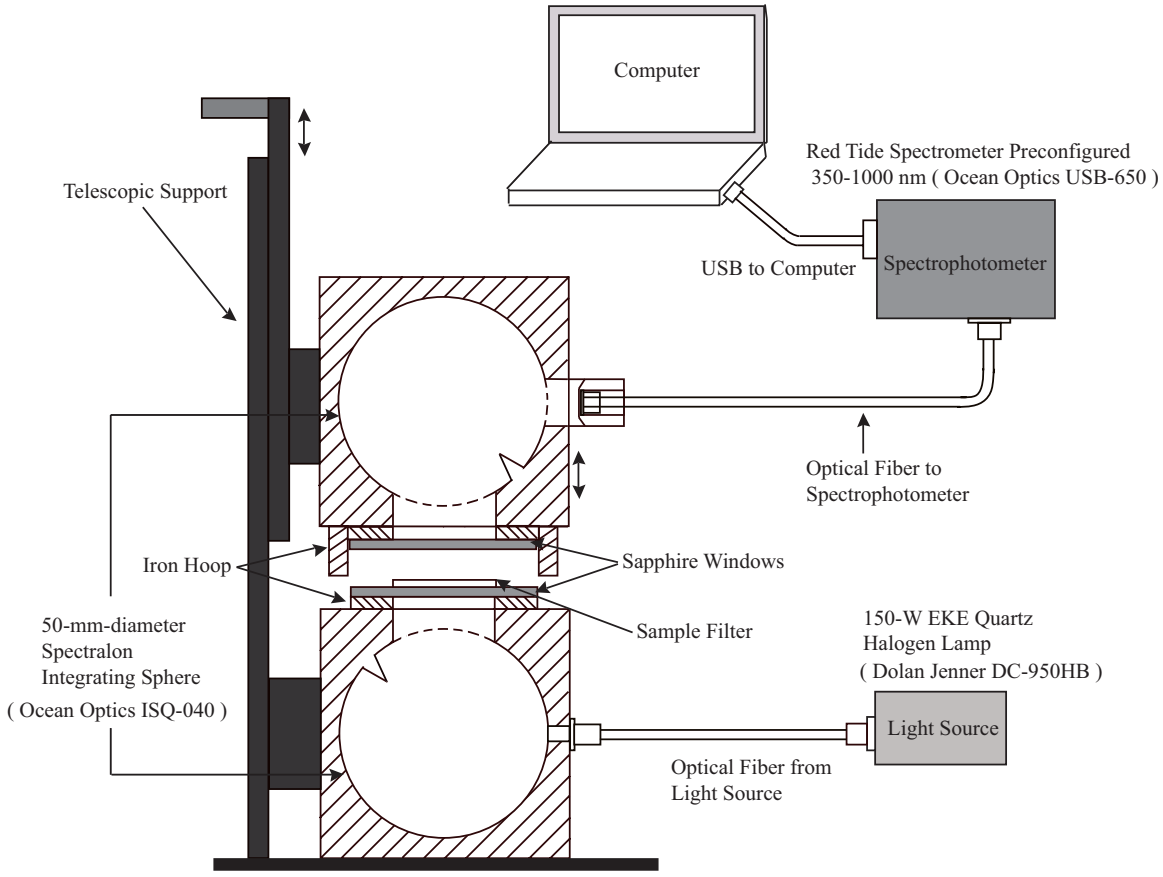

Figure 2 Schematic diagram of the improved two-sphere integrating spectrophotometer.

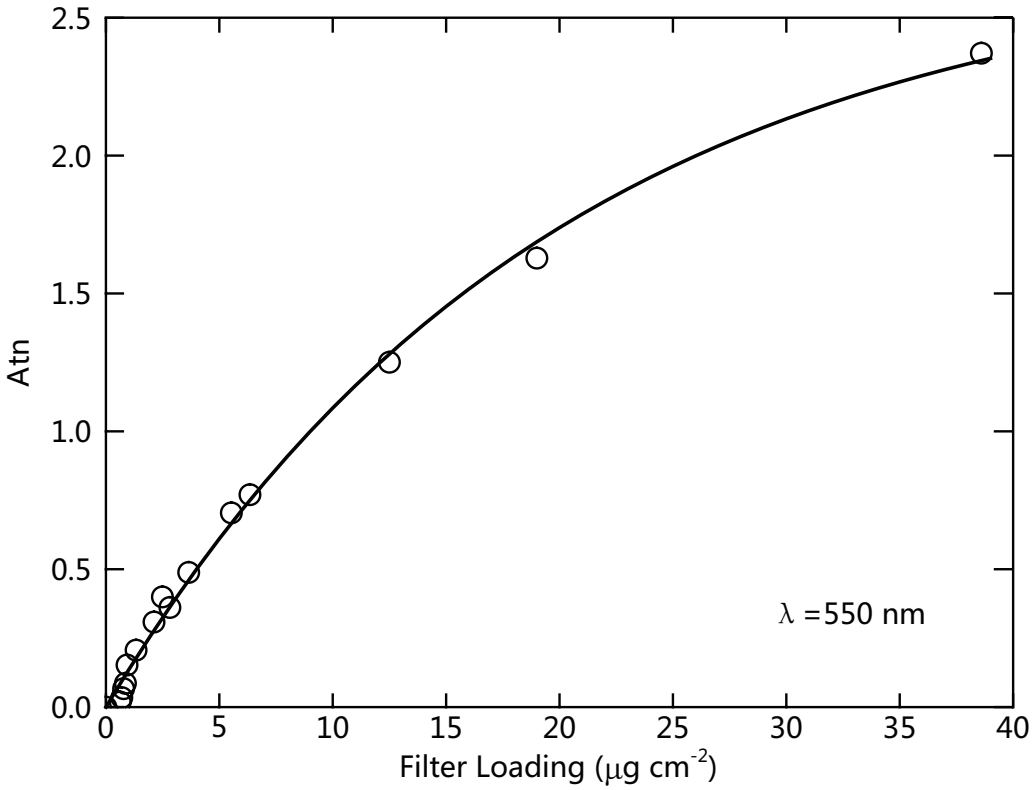

Figure 3 Calibration curve for standard fullerene soot at a wavelength of 550 nm. The solid line is a best-fit curve for the filter measurements. S_0 and S are the detected signals for the blank and sample filters, respectively, and $-\ln(S/S_0)$ is the relative attenuation.

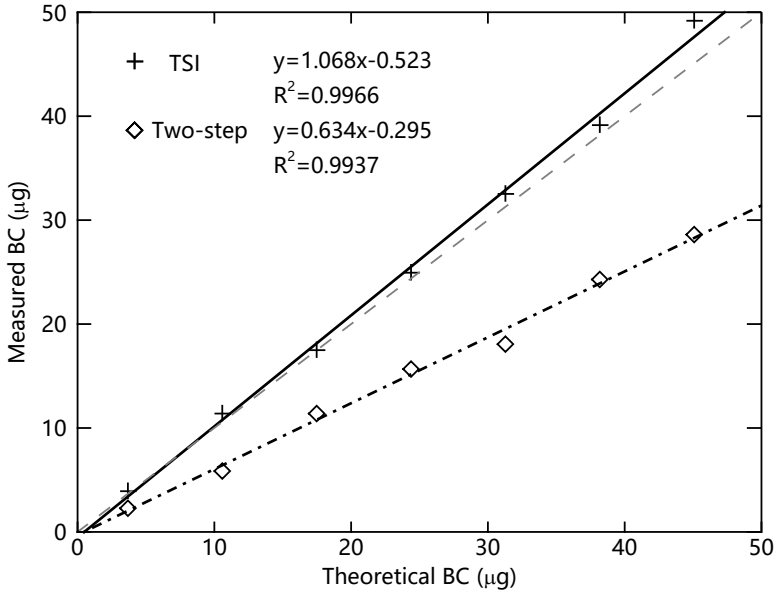

Figure 4 Comparison of the theoretical and measured BC mass determined by the TSI and two-step techniques in the laboratory. The solid and dot–dashed lines represent best-fit lines for the TSI and two-step techniques, respectively. The dashed line is a 1:1 line.

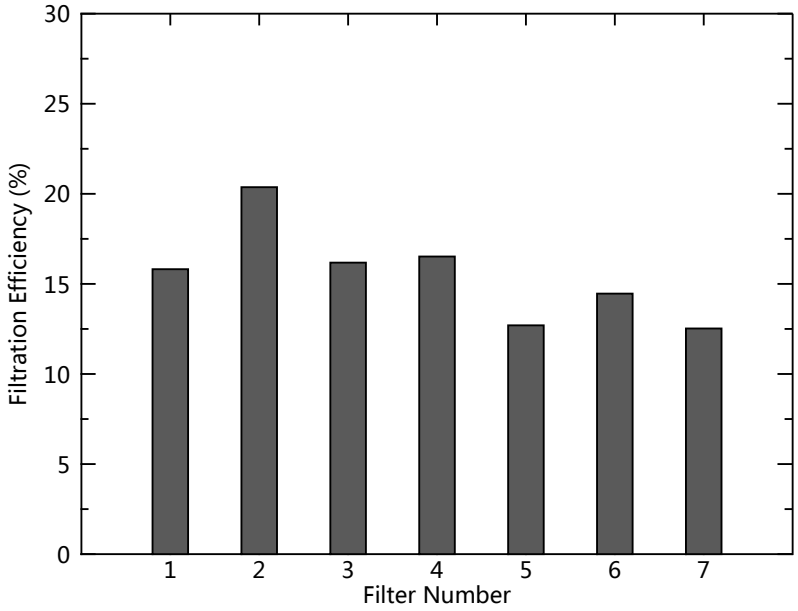

Figure 5 Mass loss of standard fullerene soot on 1.0-μm quartz fiber filters determined by refiltration using 0.4-μm Nuclepore filters.

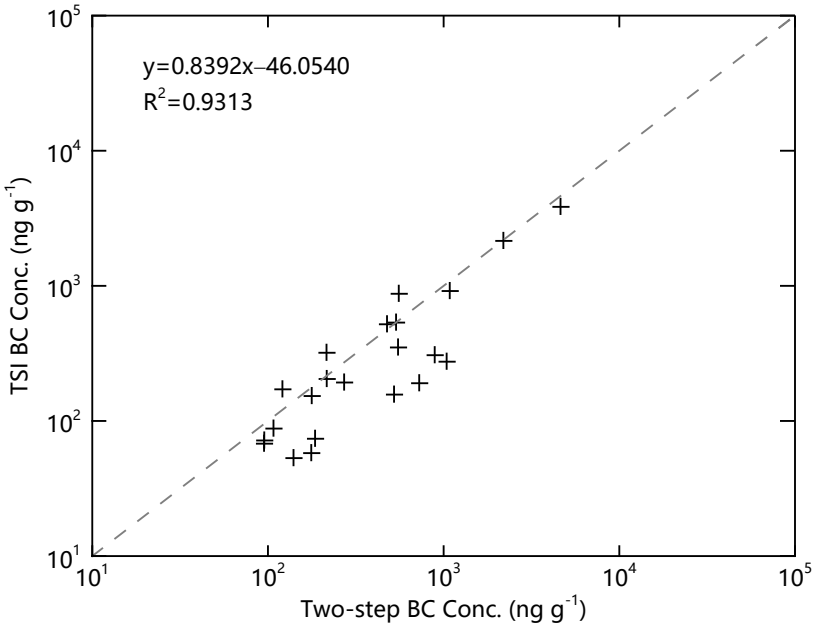

Figure 6 Comparison of BC concentrations in snow samples over northeast China during January–February 2014 determined by the TSI and two-step thermal optical methods. A 1:1 line (dashed) is shown.

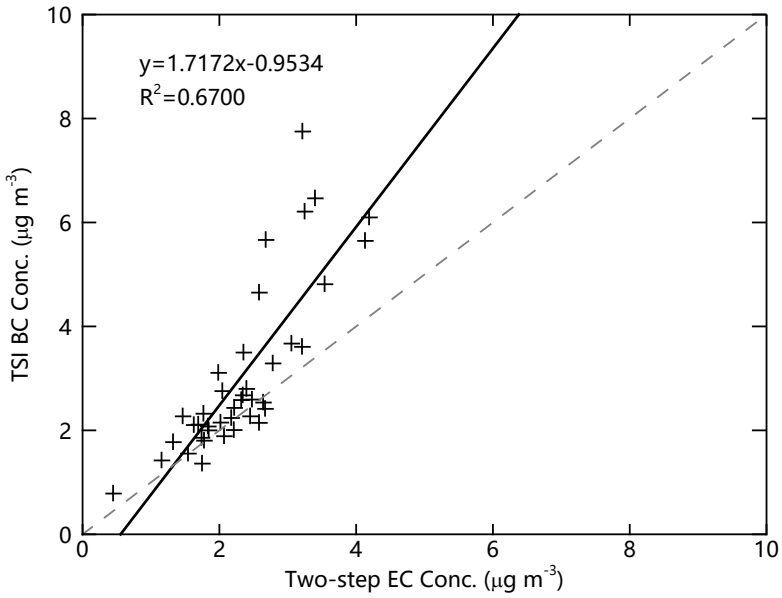

Figure 7 As for Fig. 6, but for atmospheric samples collected at Lanzhou in northwest China during 5–25 August 2015. A 1:1 line (dashed) and a linear regression fit passing through the origin (solid curve) are also shown.

873 **Table 2** Statistics of BC and EC concentrations measured using the TSI and two-step
874 thermal–optical methods for snow samples during the experiments over northern China.
875

Site	Filter	TSI BC	Two-step EC
		ng g^{-1}	ng g^{-1}
90	Q-351L	349.95	550.19
91	Q-352L	171.46	120.87
	Q-352R	152.94	177.48
92	Q-354L	53.10	139.78
	Q-354R	57.82	176.41
93	Q-356L	71.71	95.27
	Q-356R	73.85	185.45
94	Q-358L	274.62	1040.20
95	Q-359L	87.84	107.51
	Q-359R	67.92	95.01
96	Q-363L	319.71	215.42
	Q-363R	192.60	271.42
97	Q-366L	204.47	216.04
	Q-366R	306.75	889.54
98	Q-369L	1605.95	130.36
	Q-369R	1321.69	6004.33
99	Q-376L	873.58	555.39
	Q-376R	534.70	536.11
100	Q-380R	519.47	476.14
101	Q-384R	3843.15	4626.72
102	Q-388L	915.59	1083.24
	Q-388R	2151.18	2187.90
103	Q-397L	156.76	522.07
	Q-397R	190.24	726.08

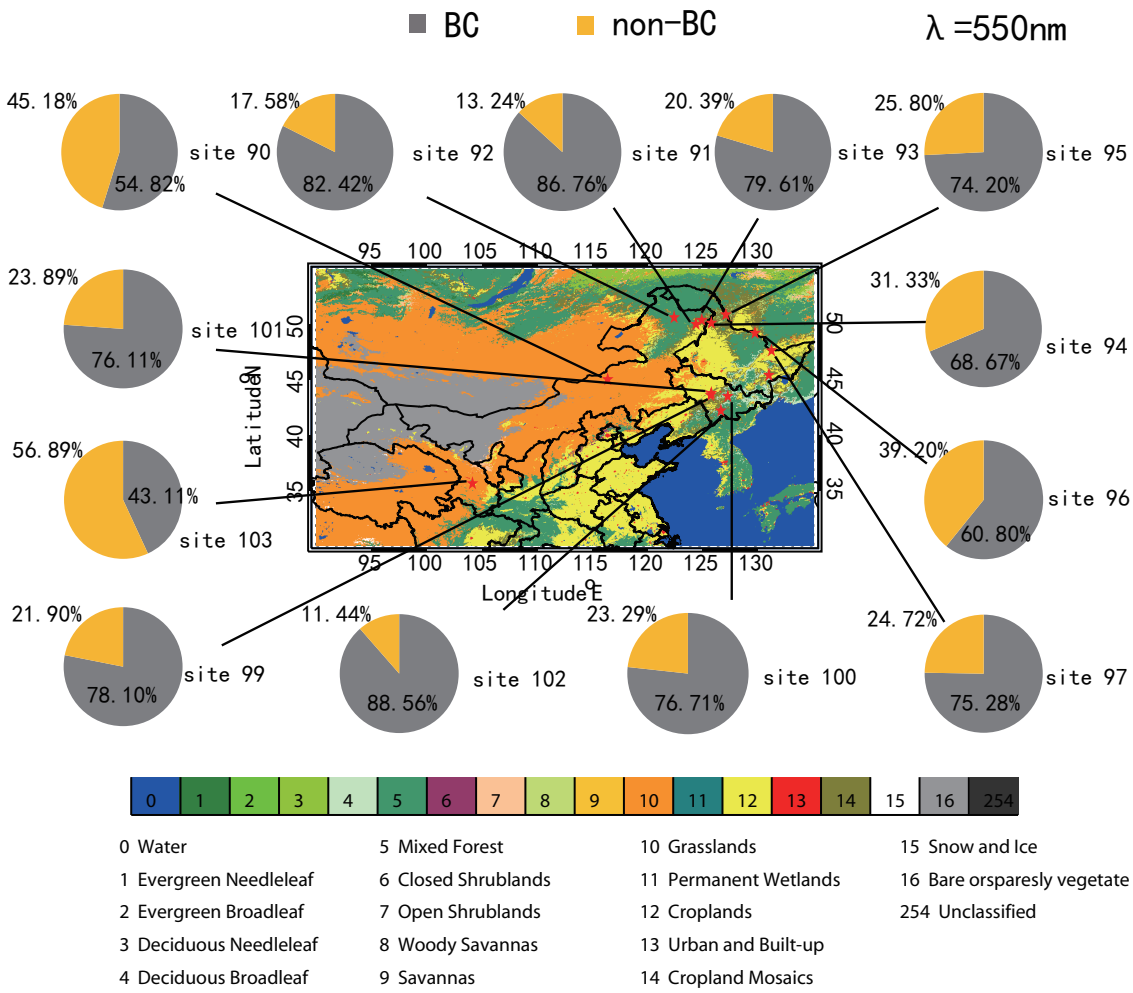

Figure 8 Spatial distributions of light absorption at 550 nm due to BC and non-BC fractions in surface snow across northern China during January–February 2014.

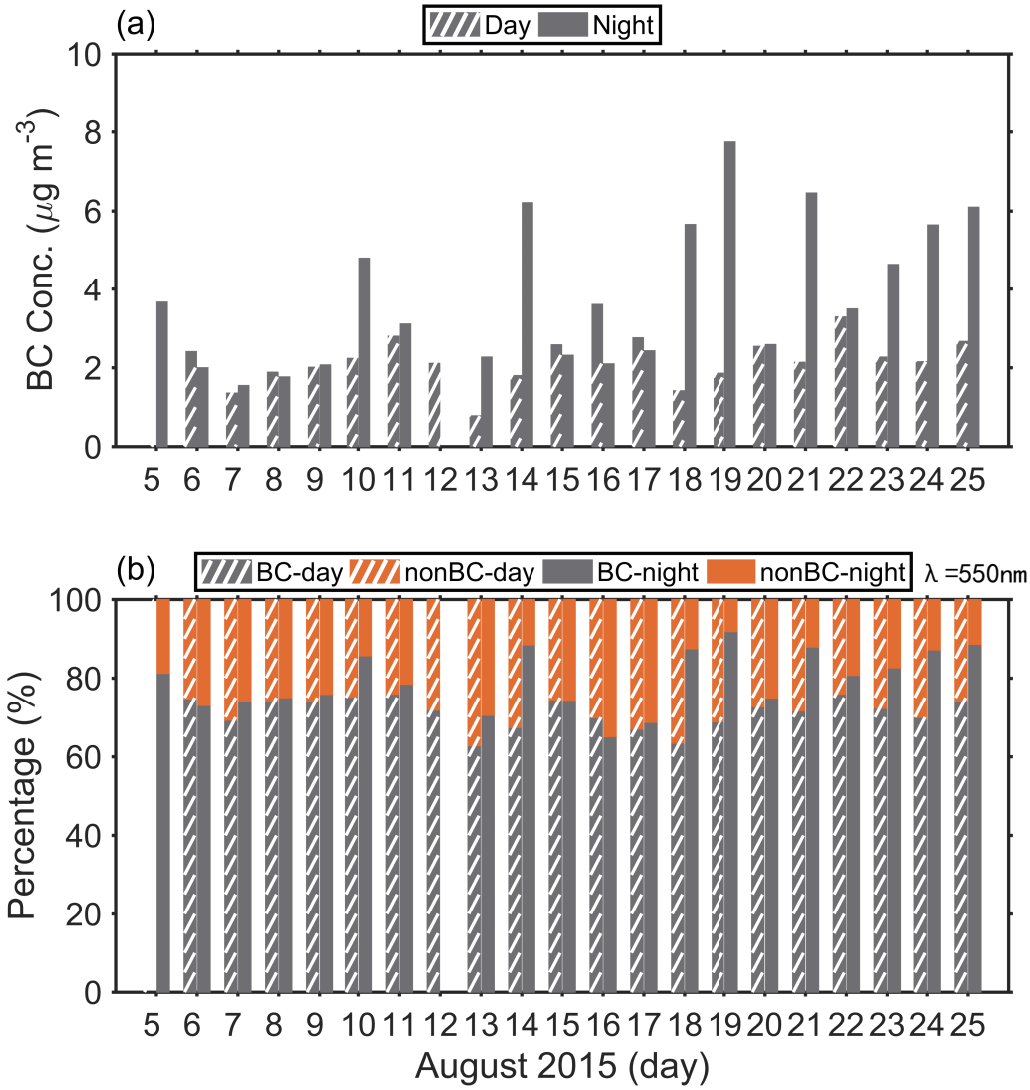

Figure 9 Variations in 8-hour **(a)** BC concentration and **(b)** BC and non-BC light absorption measured by TSI spectrophotometer at 550 nm at Lanzhou during 5–25 August 2015 (day: 9 am to 5 pm; night: 11 pm to 7 am).

889

890 **Table 3** Statistics of BC and EC concentrations in atmospheric samples measured using
891 the TSI and two-step thermal–optical methods.

Day			Night		
Date	TSI BC	Two-step EC	Date	TSI BC	Two-step EC
	μg m^{-3}	μg m^{-3}		μg m^{-3}	μg m^{-3}
2015.8.6	2.41	2.67	2015.8.5-8.6	3.67	3.05
2015.8.7	1.36	1.75	2015.8.6-8.7	2.00	1.84
2015.8.8	1.89	2.07	2015.8.7-8.8	1.55	1.54
2015.8.9	2.01	2.21	2015.8.8-8.9	1.77	1.32
2015.8.10	2.24	2.17	2015.8.9-8.10	2.07	1.83
2015.8.11	2.80	2.40	2015.8.10-8.11	4.81	3.54
2015.8.12	2.11	1.69	2015.8.11-8.12	3.11	1.98
2015.8.13	0.78	0.45	2015.8.13-8.14	2.27	1.46
2015.8.14	1.80	1.78	2015.8.14-8.15	6.21	3.25
2015.8.15	2.58	2.32	2015.8.15-8.16	2.32	1.77
2015.8.16	3.61	3.21	2015.8.16-8.17	2.10	1.63
2015.8.17	2.76	2.04	2015.8.17-8.18	2.43	2.22
2015.8.18	1.42	1.15	2015.8.18-8.19	5.66	2.68
2015.8.19	1.86	1.74	2015.8.19-8.20	7.75	3.21
2015.8.20	2.54	2.64	2015.8.20-8.21	2.59	2.48
2015.8.21	2.14	2.58	2015.8.21-8.22	6.46	3.40
2015.8.22	3.29	2.78	2015.8.22-8.23	3.50	2.35
2015.8.23	2.27	2.45	2015.8.23-8.24	4.65	2.58
2015.8.24	2.15	2.02	2015.8.24-8.25	5.65	4.13
2015.8.25	2.67	2.34	2015.8.25-8.26	6.10	4.19

892

893